

Marine Atmospheric Boundary Layer Height over the Eastern Pacific: Data Analysis and Model Evaluation

XUBIN ZENG AND MICHAEL A. BRUNKE

Department of Atmospheric Sciences, The University of Arizona, Tucson, Arizona

MINGYU ZHOU

Department of Atmospheric Sciences, The University of Arizona, Tucson, Arizona, and National Research Center for Marine Environmental Forecasts, State Oceanic Administration, Beijing, China

CHRIS FAIRALL

NOAA/Environmental Technology Laboratory, Boulder, Colorado

NICHOLAS A. BOND

NOAA/Pacific Marine Environmental Laboratory, Seattle, Washington

DONALD H. LENSCHOW

National Center for Atmospheric Research, Boulder, Colorado

(Manuscript received 16 April 2003, in final form 16 February 2004)

ABSTRACT

The atmospheric boundary layer (ABL) height (h) is a crucial parameter for the treatment of the ABL in weather and climate models. About 1000 soundings from 11 cruises between 1995 and 2001 over the eastern Pacific have been analyzed to document the large meridional, zonal, seasonal, and interannual variations of h . In particular, its latitudinal distribution in August has three minima: near the equator, in the intertropical convergence zone (ITCZ), and over the subtropical stratus/stratocumulus region near the west coast of California and Mexico. The seasonal peak of h in the ITCZ zone (between 5.6° and 11.2°N) occurs in the spring (February or April), while it occurs in August between the equator and 5.6°N.

Comparison of these data with the 10-yr monthly output of the Community Climate System Model (CCSM2) reveals that overall the model underestimates h , particularly north of 20°N in August and September. Directly applying the radiosonde data to the CCSM2 formulation for computing h shows that, at the original vertical resolution (with the lowest five layers below 2.1 km), the CCSM2 formulation would significantly underestimate h . In particular, the correlation coefficient between the computed and observed h values is only 0.06 for cloudy cases. If the model resolution were doubled below 2.1 km, however, the performance of the model formulation would be significantly improved with a correlation coefficient of 0.78 for cloudy cases.

1. Introduction

The atmospheric boundary layer (ABL) couples ocean surface processes with clouds and convection over the eastern Pacific [e.g., the stratus/stratocumulus region along the west coast of California and Mexico, the cold tongue–intertropical convergence zone (ITCZ) complex, and the southeastern Pacific stratocumulus region]. Ocean surface fluxes are determined by ocean surface temperature as well as near-surface air temper-

ature, humidity, and wind speed, all of which are explicitly linked to marine ABL processes. Over the stratocumulus region, the ABL is directly affected by entrainment processes that are linked to cloud-top radiative and evaporative cooling, while the character and the amount of clouds are also closely connected to the marine ABL structure (e.g., Albrecht et al. 1995; Stevens et al. 2003). Over the ITCZ region, convective updrafts, which typically grow upward from the marine ABL, tend to reduce ABL depth, while convective downdrafts strongly affect the thermodynamical structure of the ABL (e.g., Randall et al. 1998).

A realistic representation of ABL processes has been

Corresponding author address: Xubin Zeng, Department of Atmospheric Sciences, The University of Arizona, Tucson, AZ 85721.
E-mail: zeng@atmo.arizona.edu

recognized to be an essential ingredient of atmospheric and atmosphere–ocean coupled models. For instance, the systematic errors in the simulation of the seasonal cycle over the eastern Pacific in coupled models are related to the poor representation of marine ABL processes (including ABL clouds; Mechoso et al. 1995). Hong and Pan (1996) and Beljaars and Viterbo (1998) have also shown the significant impact of ABL processes on weather forecasting.

The nonlocal turbulence scheme based on Troen and Mahrt (1986) is one of the most widely used ABL schemes, even though progress has been made in developing more sophisticated ones (e.g., Grenier and Bretherton 2001; Lappen and Randall 2001). The nonlocal scheme has been used in the National Center for Atmospheric Research (NCAR) Community Climate Model (CCM3; Holtslag and Boville 1993; Vogelesang and Holtslag 1996), in the National Centers for Environmental Prediction (NCEP) medium-range forecasting model (Hong and Pan 1996), and in the forecasting model at the European Centre for Medium-Range Weather Forecasts (ECMWF; Beljaars and Viterbo 1998). One of the crucial elements of this scheme is the determination of ABL height (h), which is also linked to the maintenance of low-level clouds: if h is too low, the boundary layer is decoupled from the cloud layer, which inhibits the vertical transport of heat, moisture, and turbulent kinetic energy from the ocean surface to the cloud layer, and may accelerate the dissipation of clouds; if h is too high, cumulus clouds, rather than stratiform clouds, would form. For instance, a relatively small change in the diagnostic equation of h is one of the major reasons for the overall improvement of the NCAR CCM3 compared with its earlier version (Kiehl et al. 1998).

While an observationally based climatology of h over global oceans is not available at present, radiosonde data from cruises during various field experiments have been used to determine h over limited oceanic regions (e.g., Bond 1992; Yin and Albrecht 2000; Johnson et al. 2001; Subrahmanyam et al. 2003). The definition of h in these observational studies tends to be intuitive and not very quantitative. For instance, h over the Indian Ocean was identified as “the height at which the first significant inversion of θ_v (virtual potential temperature) and q (specific humidity) profiles is evident” (Subrahmanyam et al. 2003).

Here we start with an objective definition of h that is applicable to clear and cloudy ABLs. We will then use radiosonde data over the eastern Pacific to document the large meridional, zonal, seasonal, and interannual variations of h . These data will then be used to evaluate the h simulated by the NCAR Community Climate System Model (CCSM2). Furthermore, we will evaluate and improve the h formulation as used in the CCSM2 by applying it to the radiosonde data directly. In the past, using lidar data from the space shuttle *Discovery* for 9 days in September 1994, Randall et al. (1998)

found that the CCM3, which is the earlier version of the atmospheric component of the CCSM2, systematically underestimates h over oceans. In contrast, using surface-based lidar data from a cruise over the central Pacific, Collins et al. (1997) showed that the average h simulated in CCM3 agrees well with the data.

2. Data and model descriptions

a. Data description

This study uses rawinsonde data from 11 cruises over the eastern Pacific Ocean from 1995 to 2001, including those from the Tropical Eastern Pacific Process Study (TEPPS; Yuter and Houze 2000, online at <http://www.atmos.washington.edu/gcg/MG/tepps/>) in 1997 and the Eastern Pacific Investigation of Climate Processes in the Coupled Ocean–Atmosphere System (EPIC; Cronin et al. 2002, <http://www.etl.noaa.gov/programs/2001/epic/>) in 2001. Figure 1 shows that these cruises cover the eastern Pacific from 30°N to 20°S and from 130°W to the west coast of the American continents. A total of more than 30 days worth of data is available from these cruises in each of the six different months (February, April, and August–November).

Most of the sounding (temperature, dewpoint, and wind) data were obtained from the NCAR Joint Office for Science Support (JOSS), which underwent a quality control process as described by Loehrer et al. (1996). Additional sounding data were obtained by N. Bond during the cruises to maintain the tropical Pacific buoys. Together, a total of 983 soundings (with a launch interval of about 2–12 h) was obtained from all cruises. We performed additional quality control by visually examining the data to eliminate anomalous points. Ten soundings were dropped because of too many abnormal or missing points. For the remaining 973 soundings, if the data at one or more heights were flagged as bad in the original data file or by our quality control process, values would be filled in. A simple linear interpolation (in temperature, absolute humidity, and wind) was used, because the vertical resolution of the data was from 5 to 20 m. Soundings with a vertical resolution of about 5 m were averaged to a resolution comparable to the 20-m resolution of earlier sondes. Finally, the data were smoothed using a 1–2–1 smoother; that is, the smoothed value at a given level was calculated as the sum of the values at a lower level multiplied by 25%, at the level of interest multiplied by 50%, and at a higher level multiplied by 25%. Sounding data below 100 m were not used because they may contain errors introduced by the presence of the ship and large lag errors (due to the finite response time of the sensors) in an environment with strong vertical gradients, such as near the surface (Connell and Miller 1995; Wang et al. 2002).

b. Model description

The NCAR Community Climate System Model consists of four complex modeling components separately

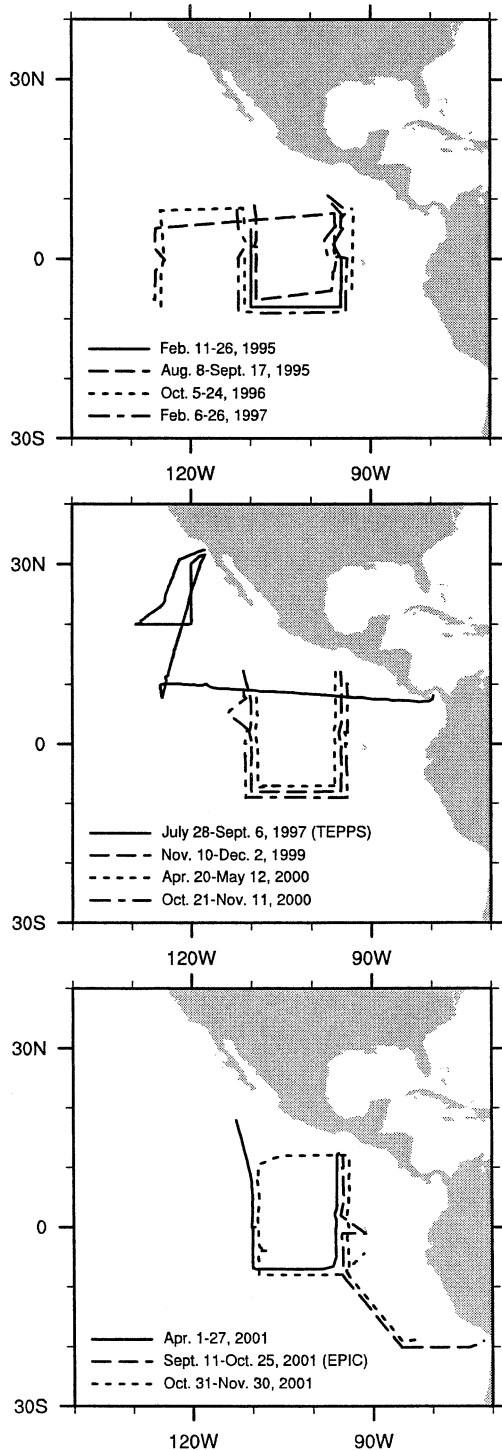


FIG. 1. The tracks, which are slightly shifted for clarity, and periods of the 11 cruises over the eastern Pacific.

simulating the earth's atmosphere, land, ocean, and sea ice, which are connected via a communication interface called the flux coupler (Blackmon et al. 2001). The ABL height, as defined in the CCSM2, is estimated as the height (starting from near surface) where the bulk Rich-

ardson number is equal to a specific critical value (Vogelezang and Holtslag 1996):

$$\frac{[g/\theta_v(z_s)](h - z_s)[\theta_v(h) - \theta_{v,s}]}{[u(h) - u(z_s)]^2 + [v(h) - v(z_s)]^2 + \beta u_*^2} = \text{Ri}_c, \quad (1)$$

where the critical Richardson number Ri_c is 0.3, z_s is the height of the first model layer above the surface, u and v are horizontal wind components, β is taken as 100, g is gravitational acceleration, θ_v is virtual potential temperature, and u_* is the friction velocity. The term $\theta_{v,s}$ in (1) for unstable conditions is

$$\theta_{v,s} = \theta_v(z_s) + 8.5 \frac{\overline{(w'\theta'_v)_s}}{w_m}, \quad (2)$$

where $\overline{(w'\theta'_v)_s}$ is the surface buoyancy flux, and w_m is a velocity scale:

$$w_m = (u_*^3 + 0.6w_*^3)^{1/3}, \quad (3)$$

with the convective velocity scale:

$$w_* = \left[\frac{g}{\theta_{v,0}} \overline{(w'\theta'_v)_s} h \right]^{1/3}. \quad (4)$$

The last term in (2) represents a temperature excess as a measure of the strength of convective thermals in the lower part of the ABL. Under stable conditions [i.e., with a negative $\overline{(w'\theta'_v)_s}$], this term is not considered in (2) and $\theta_{v,s}$ is taken as $\theta_v(z_s)$. The above formulation in the CCSM2 is the same as that in the CCM3, which is an earlier version of the atmospheric component of the CCSM2.

3. Determination of marine ABL heights from radiosonde data

Previous studies have determined h in several ways. For an unstable ABL with a capping inversion layer (or entrainment zone), the radiosonde data have been used to define h as the inversion base (Barnes et al. 1980; Albrecht et al. 1995; Gryning and Batchvarova 2002), as the height of the virtual heat flux minimum (usually in the middle of the inversion layer; Wyngaard and LeMone 1980; Sullivan et al. 1998), or as the inversion top (Betts and Albrecht 1987). In addition to radiosonde data, remote sensing data from sodar (Vogelezang and Holtslag 1996), lidar (Drobninski et al. 1998), and profiler and radar (LeMone et al. 1999) have also been used to determine h .

In order to develop an objective and quantitative definition of h based on radiosonde data, we need to consider several different situations: clear unstable ABLs [i.e., with a positive $\overline{(w'\theta'_v)_s}$], clear stable ABLs, ABLs with one layer of shallow (e.g., stratiform) clouds, ABLs with deep cumulus clouds, and ABLs with multiple layers of clouds. Based on previous studies and our interactions with various data and modeling groups, we propose to consider h as the inversion base for clear unstable ABLs. For clear stable ABLs, turbulence is gen-

erated by wind shear and possibly other processes, so that both temperature and wind data are relevant. For ABLs with one layer of shallow (e.g., stratiform) clouds, h is defined as the cloud top (usually under a capping inversion), while for ABLs with deep convection, h is defined as the cloud base. For ABLs with multiple layers of clouds, we consider h as the top of the lowest cloud layer. For the 973 soundings used in this paper, about 5% are stable in the ABL.

Following the above qualitative guidelines, a quantitative and objective criterion based on the radiosonde data is proposed as follows:

- 1) If the marine ABL is unstable, h is defined as the height (starting from near surface) where the vertical gradient of virtual potential temperature ($\partial\theta_v/\partial z$) first becomes greater than or equal to 3 K km^{-1} ;
- 2) If the ABL is stable, h is defined as the height (starting from near surface) where the bulk Richardson number first becomes greater than the critical value of 0.3 based on the criterion of Vogelezang and Holtzlag (1996) [see Eq. (1)];
- 3) If the h determined from the previous two steps lies within the cloud layer, h needs to be further adjusted as follows: if $h \geq d_c$ (cloud thickness), h is taken as the cloud top; if $h < d_c$, h is taken as the cloud base.

From the stratus/stratocumulus near the coast of California and Mexico, to the trade wind cumulus, and to the cumulonimbus over the ITCZ, the cloud top keeps increasing. The above criterion would define h as the cloud top for the stratus/stratocumulus and as the cloud base for the cumulonimbus. It would define h as the cloud base for the trade wind cumulus that is sufficiently thick (see step 3 in our criterion). This would generate an abrupt switch of h from cloud top to cloud base somewhere in the transition zone between the stratus/stratocumulus and the cumulus. If h is defined as the cloud top for the cumulus as well, the above discontinuity disappears, but a discontinuity of h would occur somewhere in the transition zone between the cumulus and deep convection. Physically, the regions of growing cumulus include vigorous updrafts over a small fraction of the area, forming at the top of the most buoyant boundary layer thermals (e.g., Stull 1988). These cumulus clouds are surrounded by a combination of clear skies and passive, decaying cumulus clouds over the remaining large fraction of the area. The weak compensating subsidence over this area effectively produces a stable layer that caps the height below which the surface fluxes are distributed. This height, which may be defined as h , is much closer to the cloud base than to the cloud top. From a modeling perspective, the computation of turbulent mixing in the ABL is closely related to h , and the impact of cumulus on atmospheric mixing is also included through a shallow convection parameterization (e.g., in the CCSM2). Therefore, our definition of h is consistent with the separate parame-

terization of turbulent and shallow convective mixings in a model.

To test the above quantitative criterion, we have selected 40 soundings with half for clear-sky and half for cloudy cases. For each sounding, the first three authors subjectively determined h (denoted as h_o) using the θ_v profile (along with the profiles of mixing ratio, relative humidity, equivalent potential temperature, and saturation equivalent potential temperature) based on the qualitative guidelines discussed earlier. The median difference between h objectively determined using the previous quantitative criterion and h_o is -11 m . The interquartile range (IQR; i.e., the difference between the 75th and 25th percentiles), which is a more robust and resistant measure of spread than standard deviations, is 72 m .

The threshold value of 3 K km^{-1} in step (i) of our criterion is admittedly somewhat arbitrary. A different value (8.3 K km^{-1}) was used over land by Bianco and Wilczak (2002). We found, however, that our estimate of h from the radiosonde data is not very sensitive to the exact threshold value. For instance, if a threshold value of 4 or 5 K km^{-1} is used, the median h using all soundings would be increased by 22 or 56 m.

Figure 2a shows a typical clear-sky sounding. The gradient $\partial\theta_v/\partial z$ first reaches the critical value of 3 K km^{-1} at a height of about 700 m, which is close to the base of the inversion capping the mixed layer. The relative humidity (RH) is less than 95% for this case. Figure 2b shows a case with the ABL decoupled from the cloud layer above. The ABL in this case is driven by surface fluxes, and its height is much lower than the altitude of the inversion that caps the cloud layer (e.g., Lambert and Durand 1999). It is also interesting to note that the air is relatively dry in the transition zone between the ABL top and the cloud base. Since the wet adiabatic lapse rate of temperature is about $3.5\text{--}5 \text{ K km}^{-1}$, $\partial\theta_v/\partial z$ will exceed 3 K km^{-1} in a well-mixed cloud. Figure 2c shows that a shallow cloud layer exists for the sounding, and indeed $\partial\theta_v/\partial z$ first reaches the critical value of 3 K km^{-1} within the clouds at about 700 m. Since the cloud thickness is less than 700 m, the cloud top at about 1000 m is defined as the ABL height. For the sounding data in Fig. 2d, $\partial\theta_v/\partial z$ also first reaches the critical value of 3 K km^{-1} within the clouds at about 600 m. However, since the cloud thickness is greater than 600 m, the cloud base at about 400 m is defined as the ABL height.

The cloud layer in Fig. 2 is taken as the layer where the relative humidity is larger than 97% as observed in broken cloud layers (Albrecht et al. 1985; Betts et al. 1995). Alternative approaches have also been suggested and debated (e.g., Chernykh and Eskridge 1996; Seidel and Durre 2003). First, we compare our cloud base with the lifting condensation level determined using the temperature and humidity data at about 100-m height for each sounding (if clouds exist). Using all sounding data, the median difference is only 16 m. To further evaluate

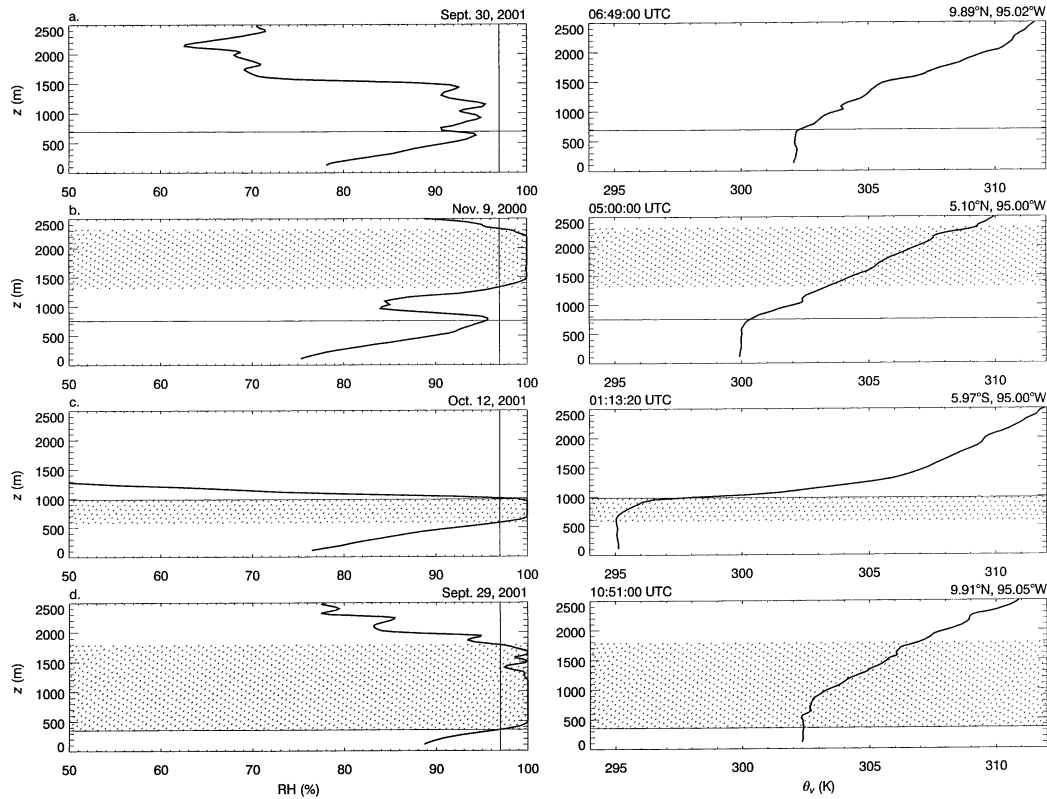


FIG. 2. Typical vertical profiles of the (left) relative humidity (RH) and (right) virtual potential temperature (θ_v) for four different situations: (a) clear sky, (b) decoupling between ABL and cloud layer, (c) thin cloud layer, and (d) thick cloud layer. Superimposed in each profile are the sounding-derived ABL height (horizontal solid line) and cloud layer (shading).

our simple approach, 3 days worth of data with stratocumulus clouds and 4 days worth of data with cumulus clouds during the EPIC experiment are used to compare the cloud layer estimated by the RH profile with the cloud base determined by ceilometer measurements and the cloud top determined by cloud radar measurements (Bretherton et al. 2003). Sounding data are available every 3 h during these 7 days. The median cloud-base difference between the RH profile method and the ceilometer measurements is -162 m, while the median cloud-top difference between the RH profile method and the cloud radar measurements is -152 m. The median difference in cloud thickness is much smaller in magnitude (-26 m). Thus, a better fit to the ceilometer and cloud radar measurements could be obtained by increasing the critical RH value of 97% at cloud base and decreasing it at cloud top. We choose not to do so because of the inherent uncertainties in using the radiosonde data to determine cloud layers (e.g., the balloon moving laterally out of the cloud layer). Furthermore, the calculation of h is not very sensitive to uncertainties in the cloud-layer determination. For instance, for these 7 days, we have computed h using the radiosonde alone and h using the radiosonde along with the cloud-base and cloud-top data provided by the ceilometer and cloud

radar, respectively. The median value and IQR of their differences are 0 and 88 m, respectively. We have also done additional sensitivity tests using all soundings and found that the median h remains the same when the critical RH value varies between 96% and 99%.

Figure 3 shows the median h for each CCSM2 grid ($2.8^\circ \times 2.8^\circ$) using data from all 11 cruises in Fig. 1 for the 6 months with a total of more than 30 days of sounding data in each month. The average and median numbers of soundings per grid cell per month are 5.4 and 3, respectively. While there are about 100 soundings over the cells centered at (7.0°N , 123.8°W) in August and (9.8°N , 95.6°W) in September, there is only one sounding on average for six different cells in each month. Just as shown in previous studies (e.g., Bond 1992), h varies with latitude. With data from multiple cruises, Fig. 3 also shows the significant variation of h with longitude and season. While h is usually high around 20°N or 20°S , the longitudes with relatively high h vary with season. While the results in Fig. 3 represent perhaps the best available temporal and spatial distribution of h over the eastern Pacific, they still cannot be regarded as the h climatology due to the scarcity of data. For the same reason, even the averaged latitudinal variation of h in Fig. 4 needs to be considered with caution.

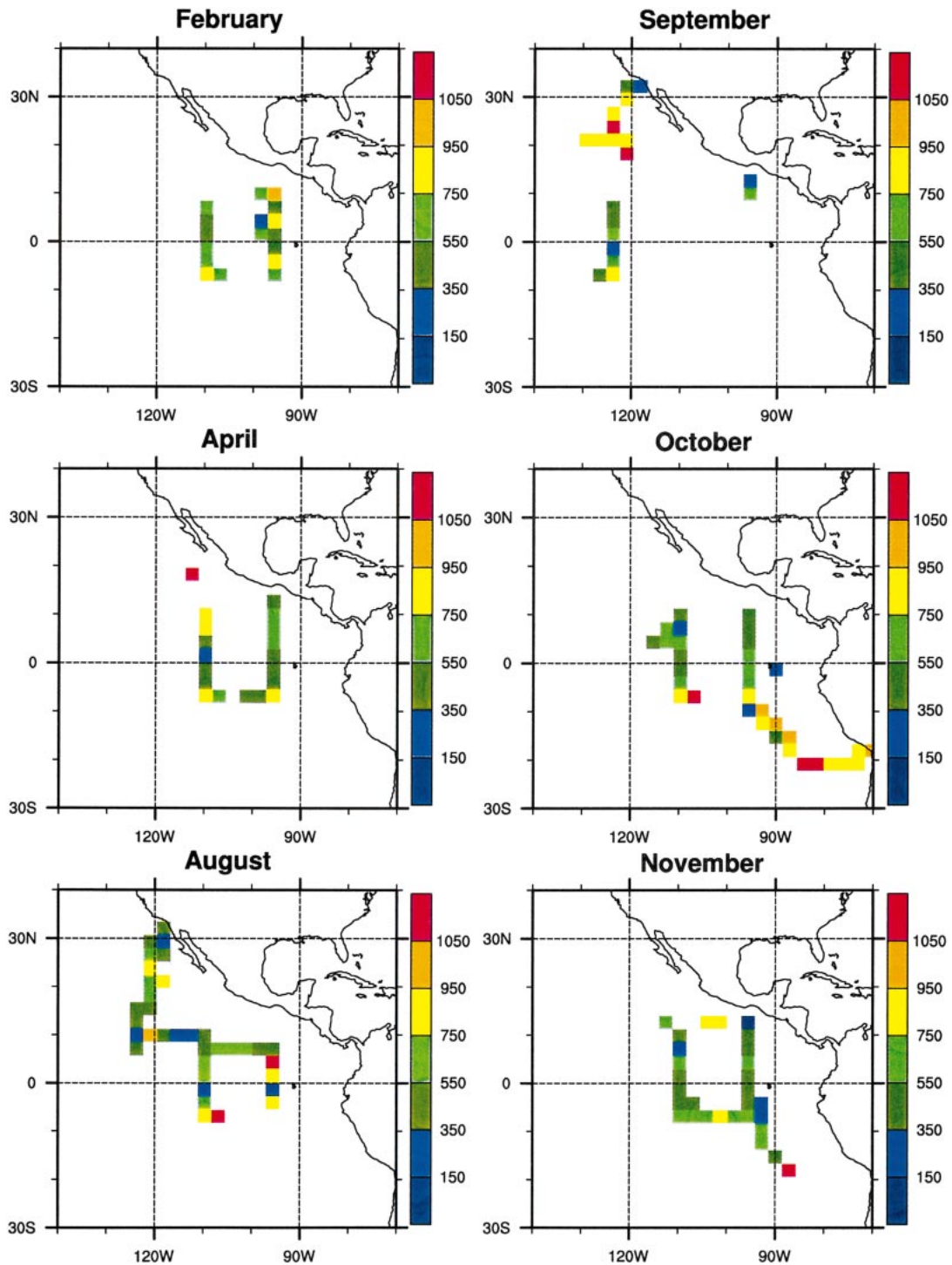


FIG. 3. The median ABL height (m) for each CCSM2 grid ($2.8^{\circ} \times 2.8^{\circ}$) using data from all 11 cruises in Fig. 1 for the 6 months with a total of more than 30 days of sounding data in each month.

Figure 4 shows the median h for each 2.8° latitude zone based on the data in Fig. 3. In February, h reaches its minimum and does not vary much from 2.8°S to 8.4°N . In April, overall h increases away from the equator between 10°S and 10°N . The latitudinal distribution

of h in August has three minima: near the equator, at the ITCZ zone, and over the subtropical stratus/stratocumulus region near the west coast of California and Mexico. There are also three peaks of h in August: over the stratocumulus region of the southeastern Pacific, be-

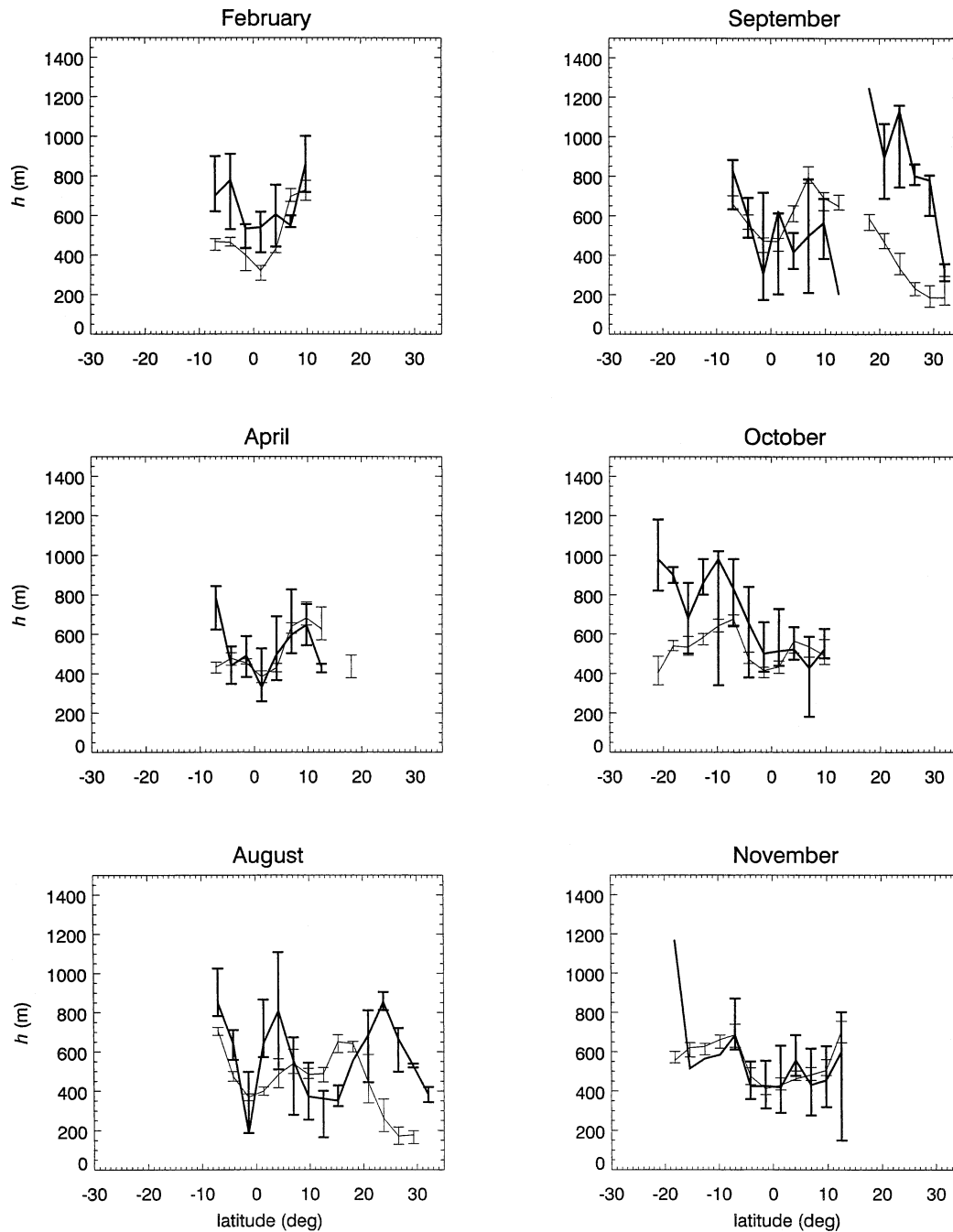


FIG. 4. The median ABL height for each 2.8° latitude zone using the same data as in Fig. 3 (denoted as thick lines) along with their interquartile ranges (i.e., the difference between the 75th and 25th percentiles, thick vertical lines). The corresponding CCSM2 results based on 10-yr model output are also shown (thin lines).

tween the equator and the ITCZ zone, and over the transition zone around 24°N between the stratocumulus and trade wind regions. The decrease of h from 24° to 12°N is not necessarily inconsistent with the increase of the trade wind inversion height (e.g., Schubert et al. 1995), because h is defined as the cloud base when the cumulus becomes deeper than h in the trade wind region. In October, h is nearly constant and reaches its minimum

between the equator and 10°N , but it increases with latitude from the equator to 10°S . In November, h does not vary much from 16.8°S to 14°N .

To see the seasonal cycle more clearly, Fig. 5 replots the data in Fig. 4 to show the seasonal variation of h at seven latitude zones (from 8.4°N to 11.2°N). Overall, the grid cell centered at 7.0°S has the highest h and has a small seasonal variation. The variation of h is also

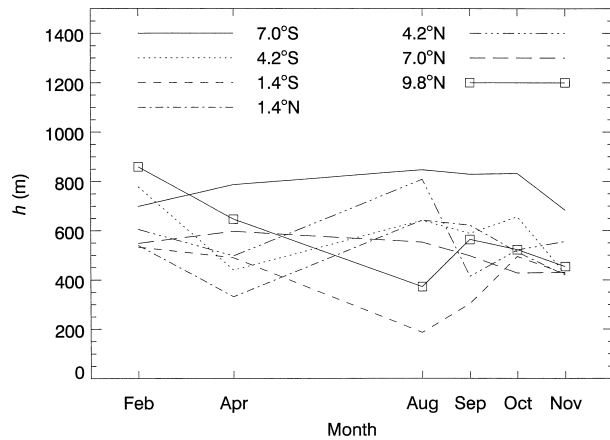


FIG. 5. The median ABL height as a function of month for the seven latitude zones (grid center latitude is shown) from 8.4°S to 11.2°N using the data in Fig. 4.

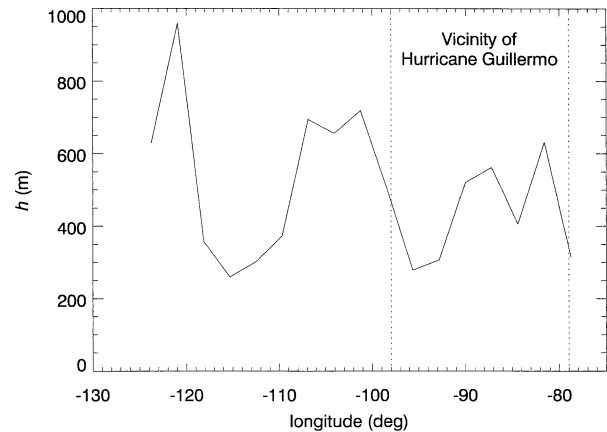


FIG. 6. The median ABL height for each 2.8° longitude zone using the data along the 10°N transect from the TEPPS cruise alone (see Fig. 1).

small at 7.0°N, but is the largest at 9.8°N. The peak of h at 7.0° and 9.8°N (in the ITCZ zone) occurs in the spring (February or April), while it occurs in August at 4.2°N and 1.4°N. The results are nearly symmetrical in the Southern Hemisphere: the peak of h at 7.0°S occurs in August, while it occurs in February at 4.2° and 1.4°S.

The scattering of data in each panel of Fig. 4 is due to the longitudinal and interannual variability of h . Figure 6 illustrates the median h for each 2.8° longitude zone using the data along the 10°N transect from the TEPPS cruise alone (see Fig. 1). Comparing Fig. 6 (from one cruise) with Fig. 4 (from all 11 cruises), the longitudinal variation of h over the eastern Pacific is as large as its latitudinal variation.

While most of the grid cells in Fig. 3 have monthly data accumulated from 1 to 2 yr only, grid cells between 8.4°S and 8.4°N along 95°W have monthly (November) data taken during 3 yr (1999–2001; Fig. 7). The sea surface temperature anomaly over the Niño-3.4 region (5°N–5°S, 170°–120°W) increased from below -1 K in November 1999 (during a La Niña event) to nearly zero in November 2001 (<http://www.cpc.ncep.noaa.gov/data/indices/>). The interannual variability of h is relatively small for the two grid cells centered at 4.2° and 1.4°S. The ABL heights at 7.0°S, 1.4°N, and 4.2°N are much higher in November 2000 than those in 1999 or 2001, while h at 7.0°N is higher in November 1999 and 2000 than in 2001.

4. Evaluation of marine ABL heights from the CCSM2

For each grid box with data in Fig. 3, we have also obtained the monthly CCSM2 ABL height output for 10 yr. Figure 4 shows the model median value for each 2.8° latitude zone (thin lines). As mentioned earlier, the sounding dataset is too small to establish anything like a climatology of h , but the model versus data comparison in Fig. 4, with the variations of the model and

observed h values represented by their interquartile ranges (IQRs), is still of some value. Model results are relatively close to observations in April and November. Overall, the CCSM2 underestimates h in February and October with some differences significant at the 95% level. In August and September, the CCSM2 significantly underestimates h north of 20°N. While the model correctly gives a local minimum of h near the equator in August and September, it does not show a minimum in the ITCZ zone (particularly in September).

It is a challenging task to understand the model versus observed h differences in Fig. 4. Here we focus on the direct testing of the h formulation as used in the CCSM2 (see section 2b). First we average the radiosonde data to the model's 26 vertical levels (denoted as L26) with the lowest five levels at about 65, 260, 631, 1225, and 2046 m, respectively. Since the radiosonde data below 100 m are not reliable, the lowest level is taken as 100 m. Compared with the h obtained from the original sounding data (with a vertical grid spacing of about 20 m) based on our objective criterion, applying the

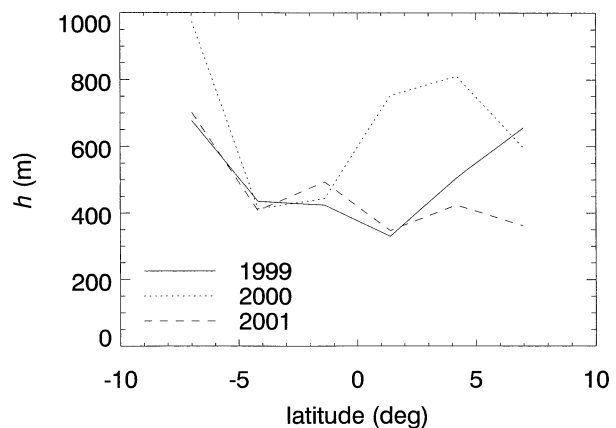


FIG. 7. The median ABL height for each 2.8° latitude zone between 8.4°S and 8.4°N along 95°W for Nov 1999–2001.

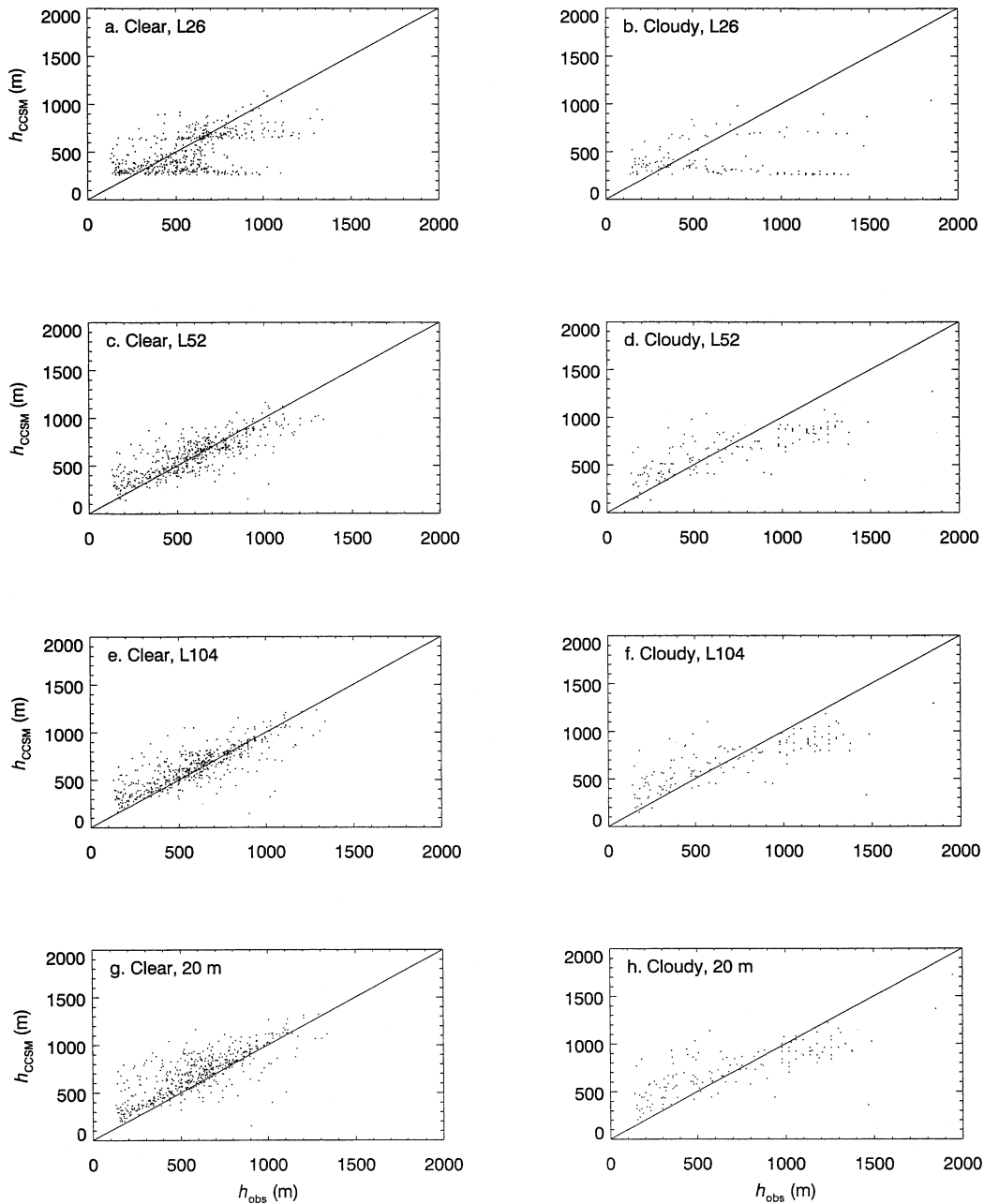


FIG. 8. Comparison of the ABL height (h) computed using the CCSM2 formulation with observed h under (left) clear and (right) cloudy conditions, respectively, using (a), (b) a model resolution with 26 layers (denoted as L26); (c), (d) doubling of model resolution (L52); (e), (f) quadrupling of model resolution (L104); and (g), (h) sounding data resolution (~ 20 m).

CCSM2 formulation to the degraded sounding data at L26 overall underestimates h under both clear and cloudy conditions, with 725 and 248 points, respectively (Figs. 8a,b). The correlation coefficients between observed and model h values are 0.48 and only 0.06 for clear and cloudy conditions, respectively. The median difference for cloudy cases is twice as large in magnitude as that for clear cases (Table 1). The IQR for

cloudy cases is as large as 792 m, which is even larger than the median observed h (of 513 m; Table 1).

Weather forecasting models usually have a higher vertical resolution than the CCSM2, and model resolution will continue to increase in the future due to increasing computer power. Therefore, we have also applied the CCSM2 formulation to the degraded sounding data averaged at three higher resolutions. By doubling the orig-

TABLE 1. The median and interquartile range (IQR) of the differences between the ABL height (h) computed using the CCSM2 formulation and the observed h , and the correlation coefficient (r) between the model and observed h values for the clear and cloudy cases (with 725 and 248 soundings, respectively). Four different vertical resolutions are tested: the original CCSM2 resolution with 26 layers (L26), doubling and quadrupling of the resolution (i.e., L52 and L104, respectively), and the sounding data resolution (~ 20 m). The median observed h values are 583 and 513 m for the clear and cloudy cases, respectively.

		L26	L52	L104	20 m
Clear	Median (m)	-73	14	38	79
	IQR (m)	290	161	128	137
	r	0.48	0.80	0.81	0.79
Cloudy	Median (m)	-153	-18	12	47
	IQR (m)	792	396	326	370
	r	0.06	0.78	0.79	0.76

inal 26 layers in CCSM2 to 52 layers (L52), the performance of the CCSM2 formulation is substantially improved (Figs. 8c,d). The median difference is less than 20 m for clear and cloudy cases and the IQRs for clear and cloudy cases are reduced by 44% and 50%, respectively (Table 1). The correlation coefficients are also substantially increased to 0.8 and 0.78 for the clear and cloudy cases, respectively. By further doubling the resolution to 104 layers (L104), the IQRs for clear and cloudy cases are further decreased, but the median difference for clear cases is actually increased. Further increasing the resolution to the data resolution of about 20 m, the median differences and IQRs for clear and cloudy cases are all increased compared with those at L104 (Table 1).

Results in Fig. 8 and Table 1 suggest that the CCSM2 formulation for computing h can be significantly improved by doubling the CCSM2's vertical resolution in the lowest 2.1 km (i.e., adding five more layers). For the original CCSM2 resolution (L26), we have also tested the use of a higher critical Richardson number (Ri_c ; e.g., as discussed in Voegelezang and Holtslag 1996). Increasing Ri_c from 0.3 (as used in the CCSM2) to 0.4, the median difference for clear cases would be reduced in magnitude by 50% to -37 m, but the correlation coefficient (r) is slightly reduced from 0.48 to 0.44, and the IQR is slightly increased from 290 to 305 m. For cloudy cases, the median difference would be reduced in magnitude by just 14% to -132 m, but r is slightly reduced and the IQR is slightly increased. Further increasing Ri_c to 0.5 would further decrease the median difference in magnitude but further decrease r for clear cases and increase the IQR.

Since the CCSM2 formulation does not explicitly consider clouds, the h computed using this formulation can be further adjusted following step (iii) in our objective criterion for data analysis (see section 3). This approach does not affect the results for clear cases, but does improve the results for cloudy cases to a certain degree: compared with the original results for L26 (see Table 1), the median difference is reduced in magnitude

by 15%, the IQR is reduced by 10%, and the correlation coefficient is increased from 0.06 to 0.16. Applying the same approach to higher resolutions also further improves the results slightly.

5. Conclusions

The atmospheric boundary layer (ABL) couples ocean surface processes with clouds and convection over the eastern Pacific, and the determination of its height (h) is crucial for ABL parameterization in weather and climate models. About 1000 soundings from 11 cruises over this region between 1995 and 2001 have been analyzed to document the spatial, seasonal, and interannual variability of h and evaluate the Community Climate System Model (CCSM2).

The definition of h in previous observational studies using radiosonde data is usually clear qualitatively but vague quantitatively. Based on these studies and our interactions with various data and modeling groups, a quantitative and objective criterion has been suggested for the determination of the height of a stable (or unstable) clear (or cloudy) ABL. The cloud base is consistent with the lifting condensation level using all sounding data. Comparing the results using this criterion with those subjectively determined by the first three authors, the median difference is only -11 m based on 40 soundings, with half for clear and half for cloudy cases. The estimation of cloud base and top is based on the relative humidity in our radiosonde data analysis. The cloud base is consistent with the lifting condensation level using all sounding data. Compared with the ceilometer measurements of cloud base and radar measurements of cloud top for 7 days, our approach underestimates the heights of cloud base and top, but these differences do not significantly affect the determination of h .

Applying this criterion to the radiosonde data over the eastern Pacific demonstrates the large meridional, zonal, seasonal, and interannual variations of h . In particular, the h distribution in August has three minima: near the equator, in the intertropical convergence zone (ITCZ), and over the subtropical stratus/stratocumulus region near the west coast of California and Mexico. There are also three peaks of h in August: over the stratocumulus region of the southeastern Pacific, between the equator and the ITCZ zone, and over the transition zone around 24°N between the stratocumulus and trade wind regions. For the seasonal variation of h , the peak of h in the ITCZ zone, between 5.6° and 11.2°N , occurs in the spring (February or April), while it occurs in August between the equator and 5.6°N . The results are nearly symmetrical in the Southern Hemisphere.

Comparison of these data with the 10-yr monthly output of the CCSM2 reveals that overall the model underestimates h , particularly north of 20°N in August and September. While the CCSM2 correctly gives a local minimum of h near the equator in August and Septem-

ber, it fails to show a minimum in the ITCZ zone, particularly in September.

Directly applying the radiosonde data to the CCSM2 formulation for computing h shows that, at the original vertical resolution (with the lowest five layers below 2.1 km), the CCSM2 formulation would significantly underestimate h . In particular, the correlation coefficient (r) between computed and observed h values is only 0.06 for cloudy cases. These results cannot be improved by increasing the critical Richardson number from the current value of 0.3 to 0.4 or 0.5, but they can be improved by adjusting the model h that falls within clouds to either cloud base for deep clouds or cloud top for shallow clouds. For instance, r would increase from 0.06 to 0.16, and the median difference between model and observed h values would be decreased in magnitude by 15%. A more significant improvement can be achieved by doubling the model resolution below 2.1 km. For instance, r would be increased from 0.06 to 0.78 for cloudy cases. Further increase in vertical resolution, however, does not significantly improve model performance.

The CCSM2 increases the number of atmospheric vertical layers from 18 (in its earlier version whose atmospheric component is the CCM3) to its current 26, but no layers were added below 2.1 km. By testing the CCSM2 formulation directly using the radiosonde data, this study suggests the need to increase the resolution below 2.1 km as well, but CCSM2 sensitivity tests are still required to further confirm the positive impact of a higher vertical resolution below 2.1 km on the overall climate modeling. The adjustment of h within clouds to cloud base or cloud top is also easy to implement in the CCSM2, and needs to be further tested as well.

Acknowledgments. This work was supported by the NOAA (NA16GP1619) and NSF (ATM0301188). Mingyu Zhou was also partially supported by the NNSFC (40233032 and 40075001) and MOST (2001DIA20026). Two anonymous reviewers are appreciated for careful reading of the manuscript and helpful comments. Suzanne Westgaard is thanked for her editorial assistance.

REFERENCES

- Albrecht, B. A., R. S. Penc, and W. H. Schubert, 1985: An observational study of cloud-topped mixed layers. *J. Atmos. Sci.*, **42**, 800–822.
- , M. P. Jensen, and W. J. Syrett, 1995: Marine boundary layer structures and fractional cloudiness. *J. Geophys. Res.*, **100**, 14 209–14 222.
- Barnes, G., G. D. Emmitt, B. Brummer, M. A. LeMone, and S. Nicholls, 1980: The structure of a fair weather boundary layer based on the results of several measurement strategies. *Mon. Wea. Rev.*, **108**, 349–364.
- Beljaars, A. C. M., and P. Viterbo, 1998: Role of the boundary layer in a numerical weather prediction model. *Clear and Cloudy Boundary Layers*, A. A. M. Holtslag and P. G. Duynkerke, Eds., Royal Netherlands Academy of Arts and Sciences, 287–304.
- Betts, A. K., and B. A. Albrecht, 1987: Conserved variable analysis of the convective boundary layer thermodynamic structure over the tropical oceans. *J. Atmos. Sci.*, **44**, 83–99.
- , C. S. Bretherton, and E. Klinker, 1995: Relation between mean boundary-layer structure and cloudiness at the R/V *Valdivia* during ASTEX. *J. Atmos. Sci.*, **52**, 2752–2776.
- Bianco, L., and J. M. Wilczak, 2002: Convective boundary layer depth: Improved measurement by Doppler radar wind profiler using fuzzy logic methods. *J. Atmos. Oceanic Technol.*, **19**, 1745–1758.
- Blackmon, M., and Coauthors, 2001: The Community Climate System Model. *Bull. Amer. Meteor. Soc.*, **82**, 2357–2376.
- Bond, N. A., 1992: Observations of planetary boundary layer structure in the eastern equatorial Pacific. *J. Climate*, **5**, 699–706.
- Bretherton, C. S., T. Uttal, C. W. Fairall, S. E. Yuter, R. Weller, D. Baumgardner, K. Comstock, and R. Wood, 2003: The EPIC 2001 stratocumulus study. *Bull. Amer. Meteor. Soc.*, **85**, 967–977.
- Chernykh, I. V., and R. E. Eskridge, 1996: Determination of cloud amount and level from radiosonde soundings. *J. Appl. Meteor.*, **35**, 1362–1369.
- Collins, W. D., J. Wang, J. T. Kiehl, G. J. Zhang, D. L. Cooper, and W. E. Eichinger, 1997: Comparison of tropical ocean–atmosphere fluxes with the NCAR Community Climate Model (CCM3). *J. Climate*, **10**, 3047–3058.
- Connell, B. H., and D. R. Miller, 1995: An interpretation of radiosonde errors in the atmospheric boundary layer. *J. Appl. Meteor.*, **34**, 1070–1081.
- Cronin, M. F., N. Bond, C. W. Fairall, J. E. Hare, M. J. McPhaden, and R. A. Weller, 2002: Enhanced oceanic and atmospheric monitoring for the Eastern Pacific Investigation of Climate Processes (EPIC) experiment. *Eos, Trans. Amer. Geophys. Union*, **83**, 205–211.
- Drobinski, P., R. A. Brown, P. H. Flamant, and J. Pelon, 1998: Evidence of organized large eddies by ground-based Doppler lidar, sonic anemometer and sodar. *Bound.-Layer Meteor.*, **88**, 343–361.
- Grenier, H., and C. S. Bretherton, 2001: A moist PBL parameterization for large-scale models and its application to subtropical cloud-topped marine boundary layers. *Mon. Wea. Rev.*, **129**, 357–377.
- Gryning, S. E., and E. Batchvarova, 2002: Marine boundary layer and turbulent fluxes over the Baltic Sea: Measurements and modeling. *Bound.-Layer Meteor.*, **103**, 29–47.
- Holtslag, A. A. M., and B. A. Boville, 1993: Local versus nonlocal boundary layer diffusion in a global climate model. *J. Climate*, **6**, 1825–1842.
- Hong, S. Y., and H. L. Pan, 1996: Nonlocal boundary layer vertical diffusion in a medium-range forecast model. *Mon. Wea. Rev.*, **124**, 2322–2339.
- Johnson, R. H., P. E. Ciesielski, and J. A. Cotturone, 2001: Multiscale variability of the atmospheric mixed layer over the western Pacific warm pool. *J. Atmos. Sci.*, **58**, 2729–2750.
- Kiehl, J. T., J. J. Hack, G. B. Bonan, B. A. Boville, D. L. Williamson, and P. J. Rasch, 1998: The National Center for Atmospheric Research Community Climate Model: CCM3. *J. Climate*, **11**, 1131–1149.
- Lambert, D., and P. Durand, 1999: The marine atmospheric boundary layer during SEMAPHORE. I: Mean vertical structure and non-axisymmetry of turbulence. *Quart. J. Roy. Meteor. Soc.*, **125**, 495–512.
- Lappen, C.-L., and D. A. Randall, 2001: Toward a unified parameterization of the boundary layer and moist convection. Part I: A new type of mass flux closure. *J. Atmos. Sci.*, **58**, 2021–2036.
- LeMone, M. A., M. Y. Zhou, C. H. Moeng, D. H. Lenschow, L. J. Miller, and R. L. Grossman, 1999: An observational study of wind profiles in the baroclinic convective mixed layer. *Bound.-Layer Meteor.*, **90**, 47–82.
- Loehrer, S. M., T. A. Edmands, and J. A. Moore, 1996: TOGA COARE upper-air sounding data archive: Development and quality control procedures. *Bull. Amer. Meteor. Soc.*, **77**, 2651–2671.
- Mechoso, C., and Coauthors, 1995: The seasonal cycle over the trop-

- ical Pacific in coupled ocean–atmosphere general circulation models. *Mon. Wea. Rev.*, **123**, 2825–2838.
- Randall, D. A., Q. Shao, and M. Branson, 1998: Representation of clear and cloudy boundary layers in climate models. *Clear and Cloudy Boundary Layers*, A. A. M. Holtslag and P. G. Duynkerke, Eds., Royal Netherlands Academy of Arts and Sciences, 305–320.
- Schubert, W. H., P. E. Ciesielski, C. Lu, and R. H. Johnson, 1995: Dynamic adjustment of the trade wind inversion layer. *J. Atmos. Sci.*, **52**, 2941–2952.
- Seidel, D. J., and I. Durre, 2003: Comments on “Trends in low and high cloud boundaries and errors in height determination of cloud boundaries.” *Bull. Amer. Meteor. Soc.*, **84**, 237–240.
- Stevens, B., and Coauthors, 2003: On entrainment rates in nocturnal marine stratocumulus. *Quart. J. Roy. Meteor. Soc.*, **129**, 3469–3493.
- Stull, R. B., 1988: *An Introduction to Boundary Layer Meteorology*. Kluwer Academic Publishers, 666 pp.
- Subrahmanyam, D. B., R. Ramachandran, K. S. Gupta, and T. K. Mandal, 2003: Variability of mixed-layer heights over the Indian Ocean and central Arabian Sea during INDOEX, IFP-99. *Bound.-Layer Meteor.*, **107**, 683–695.
- Sullivan, P. P., C.-H. Moeng, B. Stevens, D. H. Lenschow, and S. D. Mayor, 1998: Structure of the entrainment zone capping the convective atmospheric boundary layer. *J. Atmos. Sci.*, **55**, 3042–3064.
- Troen, I., and L. Mahrt, 1986: A simple model of the atmospheric boundary layer: Sensitivity to surface evaporation. *Bound.-Layer Meteor.*, **37**, 129–148.
- Vogelezang, D. H. P., and A. A. M. Holtslag, 1996: Evaluation and model impacts of alternative boundary-layer height formulations. *Bound.-Layer Meteor.*, **81**, 245–269.
- Wang, J., H. L. Cole, D. J. Carlson, E. R. Miller, K. Beierle, A. Paukkunen, and T. K. Laine, 2002: Corrections of humidity measurement errors from the Vaisala RS80 radiosonde—Application to TOGA COARE data. *J. Atmos. Oceanic Technol.*, **19**, 981–1002.
- Wygaard, J. C., and M. A. LeMone, 1980: Behavior of the refractive index-structure parameter in the entraining convective boundary layer. *J. Atmos. Sci.*, **37**, 1573–1585.
- Yin, B., and B. A. Albrecht, 2000: Spatial variability of atmospheric boundary layer structure over the eastern equatorial Pacific. *J. Climate*, **13**, 1574–1592.
- Yuter, S. E., and R. A. Houze Jr., 2000: The 1997 Pan American Climate Studies Tropical Eastern Pacific Process Study. Part I: ITCZ region. *Bull. Amer. Meteor. Soc.*, **81**, 451–481.